


RESEARCH

Open Access



Rational synthesis, characterization, and application of environmentally friendly (polymer–carbon dot) hybrid composite film for fast and efficient UV-assisted Cd²⁺ removal from water

Khoulood Jlassi^{1*} , Kamel Eid¹, Mostafa H. Sliem¹, Aboubakr M. Abdullah^{1*}, Mohamed M. Chehimi^{2*} and Igor Krupa^{1*}

Abstract

Background: Carbon dots (CDs) are of particular interest in numerous applications. However, their efficiency for heavy metal removal from wastewater was not yet reported. Herein, we rationally synthesized CDs from petroleum coke waste via hydrothermal treatment in the presence of ammonia.

Results: This drove the formation of outstanding photoluminescent, water-soluble, biocompatible, and high yield of monodispersed sub-5 nm CDs. The CDs are co-doped with high 10% of N and 0.2% of S. The as-prepared CDs possess unprecedented photoluminescent properties over broad pH range making these dots unique efficient pH sensor.

Conclusions: Chitosan (CH)–CDs hybrid hydrogel nanocomposite film was further prepared as a platform membrane for the removal Cd²⁺ metal from wastewater. The as-prepared CH–CDs membranes show relatively good mechanical properties, based on stress resistance and flexibility to facilitate handling. The equilibrium state was reached within 5 min. Intriguingly, the UV-light illuminations enhanced the Cd²⁺ removal efficiency of the photoluminescent CDs substantially by four times faster under. It was found that adsorption followed pseudo-second-order kinetic and Langmuir isotherm models. The maximum adsorption capacity at 25 °C was found to be 112.4 mg g⁻¹ at pH 8. This work paves the way to new applications of CDs in water treatment.

Keywords: Waste management, Water-soluble carbon dots, Polymer–carbon dot-based hybrid composite film, UV-assisted Cd²⁺ removal

Background

Water is the main crucial component of human life. Nevertheless, the worrying augmentation in pollution matters because of the inappropriate disposal of hazardous chemical wastes from industries [1, 2] has led to severe

negative impacts on human health and environment [3]. Thus, there is a massive demand for appropriate water purification methods to address water pollution issues [4]. The approach must usually be holistic and requires both science and technology on the one hand and environmental management, on the other hand. As part of the holistic problem solving, it is essential to design low-cost adsorbents for the effective removal of hazardous pollutants from wastewater [5]. In this regard, zeolites [6], clay minerals [7] and carbon-based materials [8] are among the most employed adsorbents for the removal of

*Correspondence: khoulood.jlassi@qu.edu.qa; abubakr_2@yahoo.com; mmchehimi@yahoo.fr; igor.krupa@qu.edu.qa

¹ Center for Advanced Materials, Qatar University, P. O. Box 2713, Doha, Qatar

² Université Paris Est, ICMPE (UMR7182), CNRS, UPEC, 94320 Thiais, France

pollutants due to their high surface area. Recently, carbon dots (CDs) were recently used as efficient adsorbents for heavy metal removal from wastewater [9]. These quantum dots, with particle size smaller than 10 nm, have emerged among the most fluorescent nanomaterials [10]; actually, they are coined “nanolights” [11]. Their success story is due to their easy preparation, low cost, high photoluminescent properties (PL), thermal stability relatively non-toxic nature and facile functionalization [12]. These salient features of CDs led to their numerous applications in sensors [13], cell imaging [14], metal detection [15, 16], organophosphate pesticide detection, light-emitting devices [17] and to name but a few [18–20]. Several protocols such as arc discharge [21], microwave digestion [22], ultrasonic oscillation [23], electrochemical method [24], hydrothermal synthesis [25] have been reported for the synthesis of CDs. Compared to previously reported protocols, hydrothermal method is the most used for its simplicity, soft conditions and great quantum yield [26].

Newly, hydrothermal treatment of many natural carbon sources [27, 28] has been fruitfully used to synthesize fluorescent CDs. Using natural carbon resources, for low cost and ecofriendly synthesis of CDs, is becoming one of the trends of CDs research. Particularly, petroleum coke, which is produced in hundreds of tons as a byproduct during the oil refining process in many oil states (Additional file 1: Tables S1, S2), has a relatively low price [29]. Thus, one can take benefit of these waste products to recycle them to design “new carbon nanomaterials of interest” with high added value. These materials can be rich in benzene rings or aromatic domains and contain a graphene-like structure (Additional file 1: Table S3); therefore, herein, we used it to prepare highly fluorescent and water-soluble CDs. Several studies reported direct relationship between the fluorescence quenching, increase of absorbance and subsequent complexation at high concentration of heavy metal ions including Pb^{2+} , Cu^{2+} and Cd^{2+} [30].

Previous studies described the feasibility of combining CDs with metallic nanomaterial or polymer matrix [31], without compromising their fluorescence [32]. There have been few reports describing the introduction of CDs in hydrogels for different emergent applications [33, 34]. Among them, chitosan-based hydrogels could be used as a host platform for green carbon dots immobilization [35–37], due to their unique properties such as biocompatibility, non-toxicity, and biodegradability [35, 38, 39]. Chitosan solubilization, happens in acidic aqueous solution, through NH_2 functional group protonation. This makes chitosan water-soluble natural polymers of major interest for making thin films and hydrogels [40].

Despite the significant progress in the fabrication of various CDs for myriad applications [41], their activity

toward UV-assisted heavy metal removal, from wastewater was not yet reported; moreover, the chemical doping of N-atom and S-atom into the conjugated carbon skeleton structure of CDs, modulated its electronic, surface chemical properties, and PL, which are greatly required merits for efficient and selective detection and removal of several metal ions [42].

In pursuit of this aim, herein, we present for the first time a simple and facile approach for controlled synthesis of CDs from petroleum coke waste via hydrothermal treatment followed by ammonia treatment. This led to the conversion of non-environmental benign petroleum coke into CDs with high benefits in many ecofriendly applications [43]. The chemical/physical properties of these novel N,S-doped CDs were studied using a series of surface and bulk characterization techniques including X-ray diffraction (XRD), scanning and transmission electron microscopy (SEM and TEM), atomic force microscopy (AFM), fluorescence, X-ray photoelectron (XPS), Raman, Fourier-transform infrared (FTIR) and UV/Vis spectroscopy (UV/Vis). Intriguingly, the presented method led to high-quantum yield of water-soluble, biocompatible, stable size dependent, pH-dependent photoluminescent (PL) and monodispersed sub-5 nm CDs enriched with N and S. The biocompatibility of CDs was proved via its integration with chitosan in the form of a membrane, which subsequently utilized for Cd^{2+} removal from water for a current local project [44] over a wide ranging of pH. Furthermore, the effect of the UV-light irradiation on the removal efficiency of Cd^{2+} via the fluorescent CDs was studied in addition to the mechanism as well.

Materials and methods

Chemicals and materials

Petroleum coke (PC) wastes were obtained from Qatar Petroleum (Doha, Qatar). H_2SO_4 (99.9%), HNO_3 (70%), and NH_3 (99.9%), glacial acetic acid (99%), NaOH (99.9%), and chitosan (medium molecular weight, Sigma-Aldrich),

Synthesis and purification of CDs and CH-CDs

A 4 g of petroleum coke was initially ground then dissolved in 90 mL of H_2SO_4 and 30 mL of HNO_3 (30 mL) under stirring/refluxing at 120 °C for 12 h. Then, the mixture was ten times diluted with H_2O then neutralized with ammonia followed by hydrothermal treatment in a Teflon-lined autoclave at 180 °C for 12 h. The resultant supernatant filtered and dialyzed with 3500 Da MWCO and kept for further analysis.

Chitosan-CDs membrane (CH-CDs membrane) was prepared by mixing CDs (3 wt%) with chitosan (10 wt%) in 0.1 M acetic acid under mechanical stirring at 30 °C.

Then, the resulting hydrogel was gently placed on a glass substrate and then uniformly dispensed along one side-wall of the doctor blade with a spreader height of 3 mm. The membranes were dried at 80 °C for 24 h followed by neutralization using NaOH (3 M) and washing with H₂O water several times before being dried and kept for further utilization.

Characterizations

Surface morphology of the prepared CDs was done using scanning electron microscopy (SEM) (ZEISS SUPRA), transmission electron microscope (TEM, JEM-2100 Plus, Jeol, USA) and atomic force microscopy (AFM) measurements were performed in tapping mode on a MFP 3D (AsylumResearch). Particle size was determined by DLS with 90° detection optics using a Zetasizer ZS90 (Malvern Instruments Ltd., Westborough, MA). Instrument performance was first evaluated using particle standards, singly and as binary mixtures. The X-ray photoelectron spectra XPS measurements were conducted using a Kratos Shimadzu Axis Ultra DLD machine (Kratos, Manchester, UK) equipped with a monochromatic Al K α radiation source (1486.6 eV). X-ray diffraction analysis was carried out on films using X'Pert PRO (PANalytical) diffractometer using CoK α (1.789 Å) radiation operation voltage and current was maintained at 40 kV and 200 mA, respectively, The theta interval (20–50 °C) and the analysis speed rate (0.05 °C s⁻¹). The Fourier-transform infrared spectroscopic (FTIR) studies were carried out using the FTIR Frontier (Perkin Elmer) instrument. The Raman spectroscopy was measured using an Ar+ ion laser at 514.5 nm (Renishaw inVia 2000 Raman microscope, UK), with a spectral resolution < 1.5 cm⁻¹, all the spectra were initially baseline corrected with third-order polynomial and normalized to the max of the peak intensity. UV/Vis absorption spectra were determined using UV/Vis spectrophotometer (Gold Spectrumlab 54, Shanghai Lengguang Technology Co. Ltd., China). The fluorescence spectra were performed for three samples of CDs prepared at different periods of time, using a HORIBA SPEX Fluoro-log-3-11 spectrofluorometer. No significant shifts in the fluorescence peaks were noted from batch to batch. Dynamic Mechanical Analysis: the prepared CH-CDs samples was tested using the conventional melt mixing technique were cut into rectangular shapes (50 mm/10 mm/1 mm) and were subjected to dynamic mechanical analysis (DMA) using a Perkin-Elmer DMA.

Selectivity toward heavy metal removal

The prepared CH-CDs hybrid films and pristine was tested for heavy metal removal application. To track the selectivity, the as-prepared CH and CH-CDs hybrid films

were immersed in three selected metal picrate solution; Zn(NO₃)₂, Pb(NO₃)₂ and Cd(NO₃)₂ (25 mL, 50 ppm) at room temperature, PH=8, then washed several time with diazoned water, the supernatant are characterized using ICP to determine the metal extraction rate .

Adsorption experiment

The kinetics, and isotherm parameters were calculated. CD-based chitosan membranes (100 mg) and (50 ppm, 25 mL) of Cd²⁺ solution were used, stirred (180 rpm, 30 min). The remaining cadmium was evaluated using the inductive coupled plasma (ICP) technique. All the adsorption experiments were repeated three times.

At equilibrium, the adsorption capacity, q_e (mg g⁻¹), was deduced using the Eq. (1):

$$q_e = (C_i - C_e) \times V/M. \quad (1)$$

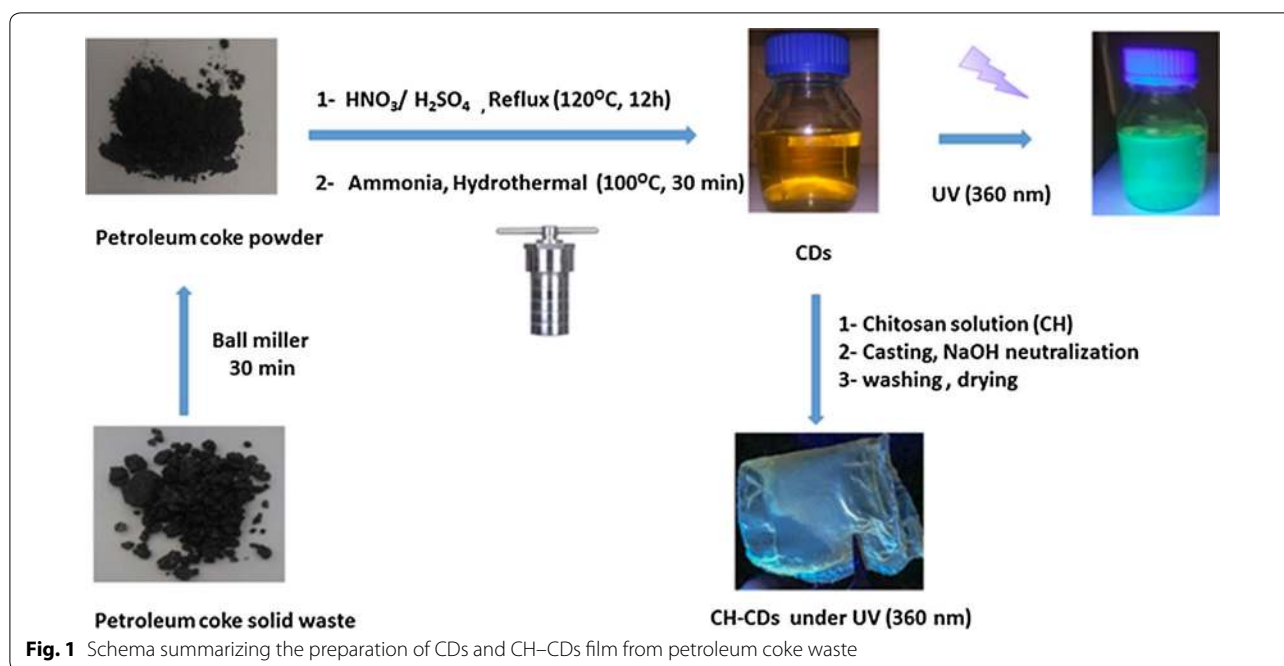
C_i and C_e (ppm) are the initial and equilibrium concentration of Cd²⁺. M (g) is the mass of adsorbent and V (L) is the volume of solution.

Results and discussion

Preparation of CDs and CH-CDs

Figure 1 is a schematic illustration of CDs and CH-CDs nanocomposite preparation. PC, as a green and cost-effective material, is used as a carbon source for preparing of fluorescent carbon dots (see Additional file 1: Table S2).

The petroleum coke has been oxidized first using HNO₃ and H₂SO₄ acids and then doped using ammonia via a hydrothermal process. The as-obtained CDs, functionalized with hydrophilic groups such as nitrogen and carboxylic groups [45], show a deep yellow color, exhibiting blue-green emission under UV light (360 nm) and excellent solubility and stability in water. No precipitation was noted even after 6 months. These prepared water-soluble CDs was impregnated with Chitosan polymeric matrix to form a membrane serving as solid and hybrid film for heavy metal complexation and exchange and to control the solubility of CDs in water solution [46]. The as-obtained film shows a blue-greenish color under UV as well. Indeed, the as-obtained CDs actuality negatively charged (zeta potential of - 16.05 mV, (Additional file 1: Figure S1) interact electrostatically with chitosan (positively charged, because its dispersion in acidic medium) with a zeta potential of + 34 mV which imparts uniform distribution and their uniform distribution in the obtained composite film. For complementary evaluation of the role of the prepared CDs in the chitosan biopolymer matrix, the mechanical properties of the chitosan/CDs nanocomposites were explored. The stress strain curves of the chitosan and chitosan/CDs nanocomposites at different concentrations of CDs are shown in

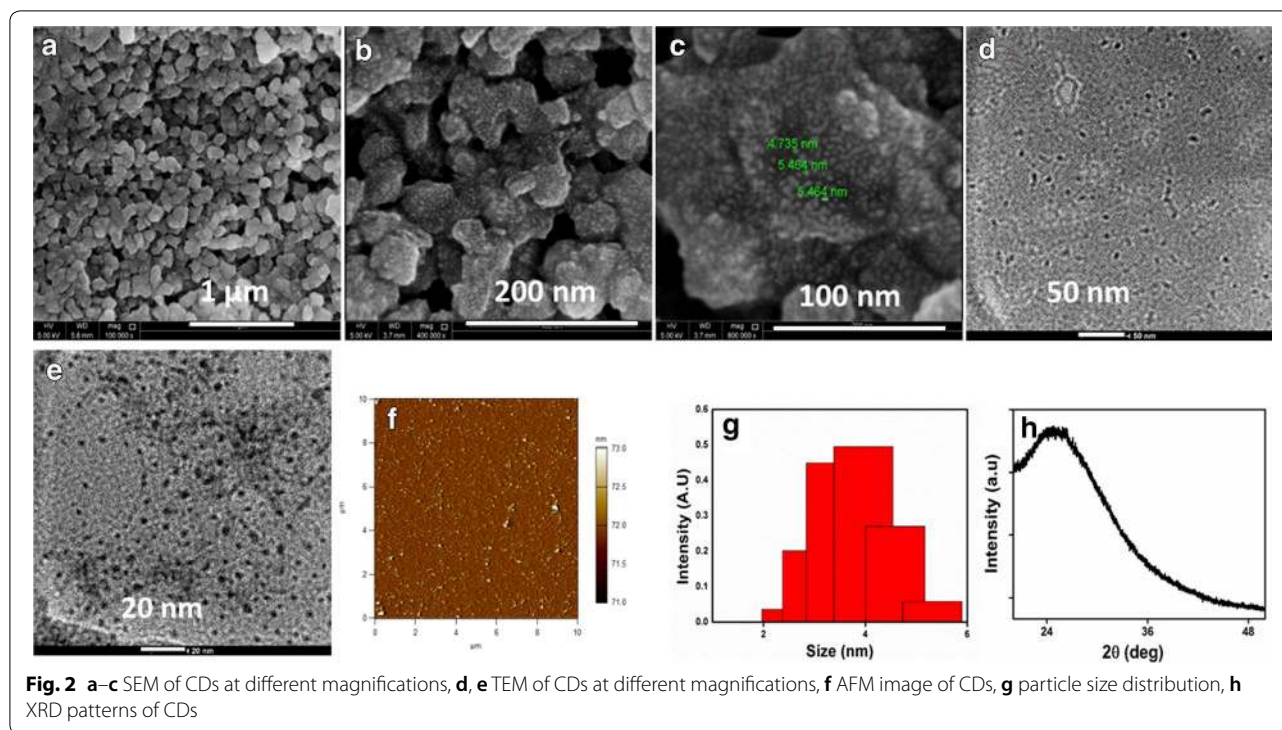


Additional file 1: Figure S2a). The mechanical properties of the nanocomposites at the concentration of 20 wt% CDs were improved compared to the pure and 5 and 10 wt% composites. It can be concluded that the concentration of 20 wt% might be chosen as the optimal concentration. The mechanical properties of the developed membranes were investigated as well by DMA Additional file 1: Figure S2b. This latter indicates better high temperature resistance along with improved properties at high temperatures for the 20 wt% sample. Moreover, the chitosan-filled CD membranes display an increase in the storage modulus over the entire E' spectrum as compared to the pristine. These features indicate a large decrease in the macromolecular motion ability of CH-CDs 20 wt% sample Additional file 1: Figure S2c.

Physical structure

Figure 2 show the SEM, TEM, AFM image, DLS and XRD of CDs, Fig. 2a–c shows the data from SEM. The diameter of spherical CDs is around 4.5 nm, and the size distribution is consistent with the Gaussian distribution (Fig. 4g). The SEM images reveal that the PC has an irregular block-like shape. Meanwhile, the typically prepared CDs were formed in a high yield of regular size and shape nanoparticles. Figure 2c shows that the nanoparticles have a spherical-like shape, with an average diameter of 4.5 nm. The dynamic light scattering (DLS) histogram (Fig. 2g) displays the monodispersing of the as-formed nanoparticles with similar size obtained by the SEM image.

The XRD analysis of CDs (Fig. 2h) exhibited one dominant diffraction peak at 2θ of 27° assigned to the facets of graphitic-like carbon. The resolved XRD peak was weak and broad, implies the small size and disordered stacking of CDs. This was emanated from the integration of both N and S into the C-skeleton structure, which results in the expansion of its lattice structure. This can be seen in the blue shift in the XRD peak relative to pure graphitic. The TEM images were carried out to further confirm the uniform structure of the as-prepared CDs. The low-magnification TEM image displays that, the CDs have uniform spherical morphology with the absence of any kind of undesired macroscopic phases such as irregular or amorphous byproducts. These CDs were monodispersed with an average size of 4 ± 0.5 nm (Fig. 2c, g). The AFM image also confirmed the uniformity of the obtained CDs (Fig. 2f) with a height of ranged from 0.5 to 5 nm (Additional file 1: Figure S3). The high AFM topographic height profile shows the average height of CDs was about 1.8 nm, demonstrating that, there are 2–4 layers of the graphitic-like nanostructure, in line with elsewhere reports [45]. The determined zeta potential of the prepared CDs (Additional file 1: Figure S1) found to be -16.05 mV which is in line with the negatively charged CD surface. Encouraged by the uniformity and small particle size of CDs, its optical properties were benchmarked using both UV–Vis and photoluminescent spectroscopy.

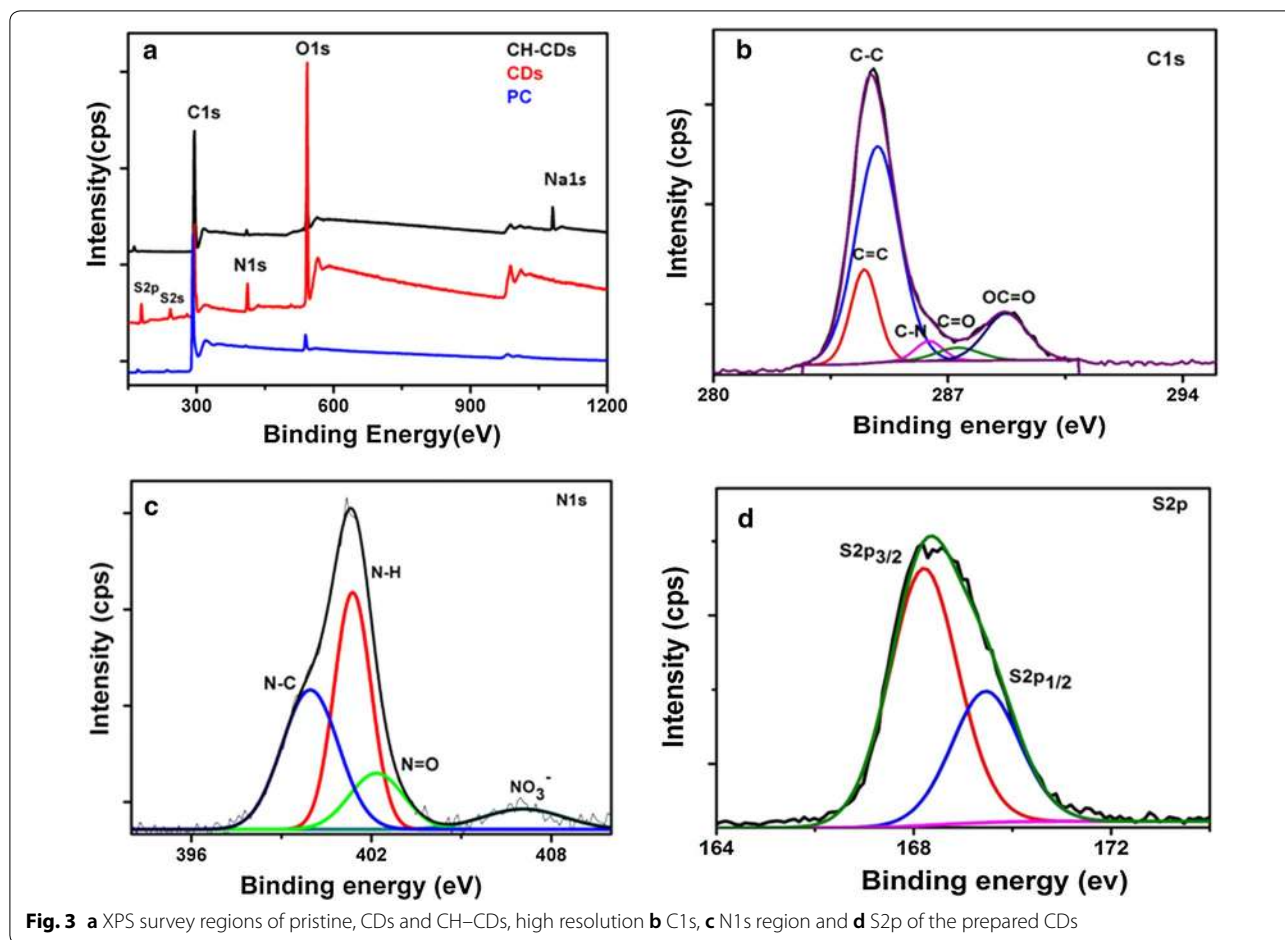


Chemical structure

The XPS was employed to explore the chemical surface composition of the used and prepared materials. The XPS survey of PC resolved the presence of C1s and O1s. Meanwhile, CDs showed C1s, O1s, S2p, and N1s, implying the formation of graphene CDs enriched with N and S (Fig. 3a). It is noteworthy that, the intensity of both C1s and O1s peak in CDs was significantly higher than their counterparts in PC, infers the high degree of surface carbon oxidation. The high-resolution XPS spectra of C 1s (Fig. 3b) exhibited C–C/C=C at 284.7 eV, and sp^2 carbon–nitrogen N–C=N at 286.5 eV, C–S 286.1 eV, and C=O at 288.3 eV. The determined percentage of sp^2 hybrid carbon atoms of CDs was found to be 89.8–93.8%, infers its high degree of graphitization. Likewise, the N1s spectra (Fig. 3c) revealed pyridinic-N (N1) at 398.6 eV, pyrrolic-N (N2) at, 400.0 eV, graphitic-N (N3) at 401.7 eV and nitrates (NO_3^-) at 407 eV, which are the omnipresent features for N-doped carbon-based materials. This indicates the successful N-doping of CDs via hydrothermal treatment in the presence of ammonia. The O1s spectra depicted two peaks at 530.1 and 532.2 eV assigned to C–O and –OH, respectively. The S 2p (Fig. 3d) doublet is fitted with two peaks originating from spin–orbit coupling, attributed to $S2p_{3/2}$ and $S2p_{1/2}$ in the 2:1 ratio; $S2p_{3/2}$ is centered at 168.5 eV and assigned to C– SO_3 –H chemical environment [47].

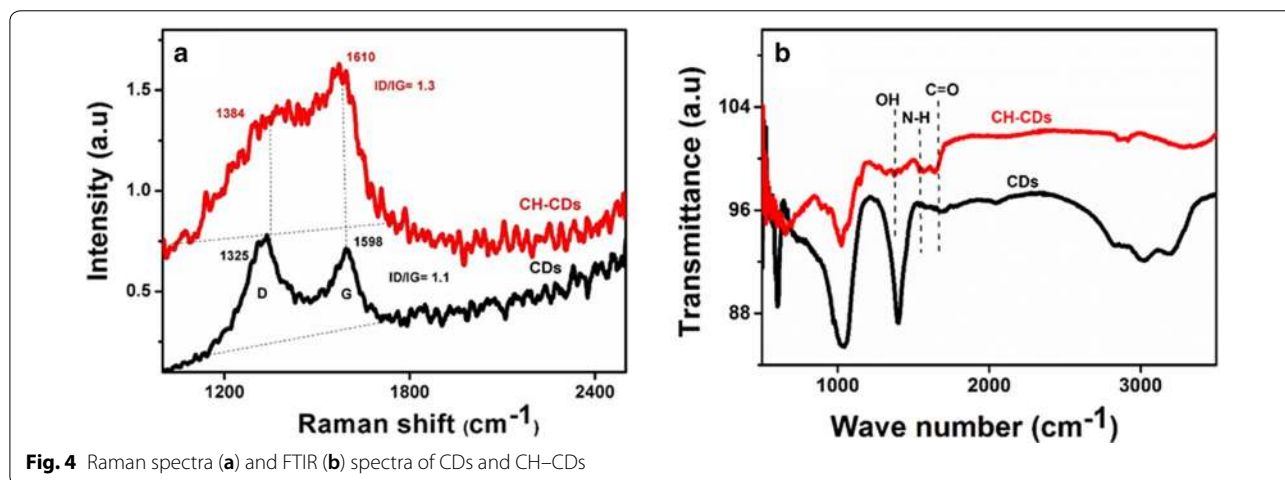
The chemical compositions (in atomic ratios) are reported for all samples in (Additional file 1: Table S4). The atomic ratio C/N/O/S is determined to be 81/10/7/2, respectively, confirming the co-doping of CDs with both N and S. The chemical doping of N-atom and S-atom into the conjugated carbon skeleton structure of CDs, modulated its electronic, surface chemical properties, and PL, which are greatly required merits for efficient and selective detection and removal of various metal ions.

The Raman spectrum of the CDs (Fig. 4a) clearly warrants the typical characteristic G band centered at 1609 cm^{-1} corresponds to the sp^2 bonded C atoms and an insignificant peak for D band at 1330 cm^{-1} ascribes to the disordered C atoms at the edges of CDs [48, 49]. The lower intensity of D band peak at 1330 cm^{-1} is owing to the high crystallinity and graphitization degree of thus obtained CDs high graphitization. This is clearly seen in the sharpness and higher intensity of G band as well as higher IG/ID ratio. The intensity of crystalline G band was substantially higher than the disordered D band, infers the formation of CDs with a great degree of graphitization and graphite-like stacking domains, in line with the XPS results. This could be further seen in the high ratio IG to ID (1.3), indicating the uniformity of the as-made CDs. Meanwhile, the slight broaden in both IG and ID, originated from the presence of both N-atom and S-atom in the C-backbone structure, which partially



disrupts the π -extended framework and originates abundant defects to the basal planes and the edges as well. On the contrary, the IG/ID of PC (1.1) was significantly smaller than CDs, implying its successful conversion to CDs. The determined IG/ID of our newly synthesized CDs was higher than previously reported works [50, 51].

The FTIR spectra of CDs (Fig. 4b) revealed obvious absorption bands centered at 1000–1400 cm^{-1} , which are attributed to the stretching vibrations of C–O, C–S and C–H, respectively [52]. Meanwhile, the bands at 2000–3500 cm^{-1} corresponded to the stretching vibrations of S–C–N, CH–, N–H, –OH, respectively [53]. This implies



the formation of carbon co-doped with N and S, agrees with the XPS results.

Optical properties of CDs

The UV–Vis absorption of CDs (Fig. 5a), displays two absorption peak centered at 230 and 285 nm, assigned to $\pi \rightarrow \pi^*$ transition of C=C and $n \rightarrow \pi^*$ transition of C=O, which similar to previously reported carbon quantum dot-based materials [47]. The low-intensity absorption shoulders of $n \rightarrow \pi^*$ is attributed to the lower content and weak electron transition of functional group such as C=O and N=O in CDs as usually noticed in the CDs prepared from industrial wastes [54]. The CDs excited at 340 nm UV light show strong greenish-blue color (Fig. 5a). Excitation-dependent PL behavior with optimized concentrations of CDs was observed (Fig. 5b), which is common for fluorescent carbon materials. The latter could be used in multi-color imaging purpose (Additional file 1: Figure S4). The emission spectra (335–500 nm range) of the CDs (Fig. 5b) show a variation in the PL intensity as the excitation wavelength varied from 360 to 500 nm. The maximum emission intensity reached 489 nm (blue emission) when it is excited at 440 nm. The size effect and the surface composition affecting the band gap of CDs are considered as reasons for the complexity of the PL behavior [55]. Intriguingly enough, the emission intensity was enhanced substantially upon inverting the excitation wavelengths. Additionally, the emissions were significantly red-shifted from 480 to 600 nm. The excitation-dependent PL behavior of the CDs is comparable to the CDs previously reported [47]. This latter could be allied with the aromatic C–C bonds and surface defects resulting from C–OH, C=O, C–S and C–N groups in the CDs. From UV data (Fig. 5a), the band gap energy of CDs was calculated using this equation [$\alpha v h = A (v h - E_g)^{1/2}$], where α , v , h , A , and E_g are the absorption coefficient, light frequency, blank constant, constant, and band gap

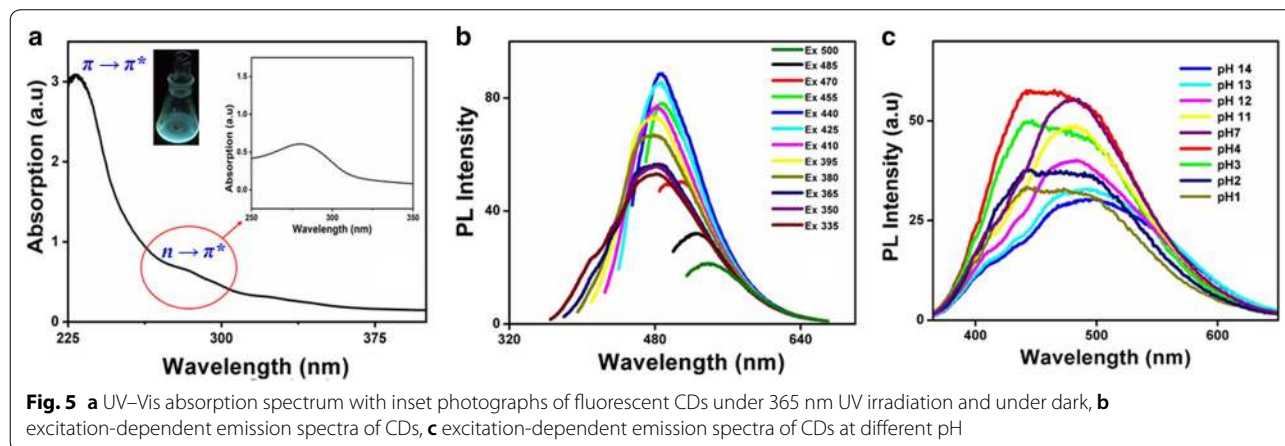
energy, respectively. The band gap of N and S doped CDs was determined to be 3.3 eV. This lower band gap (compared to the CDs without doping 3.72 eV) is emanated from the co-doping effect with both N-atoms and S-atom, agrees with elsewhere reports [56]. The effect of pH on CDs and consequently on the quenching phenomenon was explored (Fig. 5d). The emission band is slightly shifted, shows the emission can be controlled by protons. It was noted as well, that at lower pH values, the photoluminescence intensity increased, and at higher pH values, the intensity decreased (Fig. 5c). Nevertheless, within the pH range 4–7, not a remarkable variation was noted. This pH-dependent photoluminescence behavior may be attributed to the extent of proton acceptance by the nitrogen/sulfur atoms followed by potential proton transfer from the protonated nitrogen to the conjugated carbon structure [57, 58].

Heavy metal extraction test using CH–CDs hybrid films

Few recent studies have shown the ability of CDs based composites to adsorb heavy metals from aqueous solution [59]. In this work, to investigate the selectivity toward heavy metals removal, the as-prepared CH–CDs was tested in the presence of Cd^{2+} , Zn^{2+} and Pb^{2+} at a (pH 8.0). The results showed that, the removal efficiency of CH–CDs towards Cd^{2+} , Zn^{2+} , and Pb^{2+} were about 93, 55, and 40%, respectively, indicates the removal selectivity towards Cd^{2+} ions (see Additional file 1: Figure S5).

Influence of pH and contact time on Cd^{2+} removal

The adsorption of Cd^{2+} on (CH–CDs) hybrid films as a function of solution pH and contact time was checked. Toward this end, the CH and CH–CDs films were immersed in a 50-ppm solution of Cd^{2+} up to 30 min, under light and dark conditions and at different pH values and followed by the tracking of the remaining concentration of Cd^{2+} ion in solution by the ICP



analysis technique. More details about procedure were discussed in “Materials and methods” section. The extraction efficiency as a percentage (%E) was calculated via the following equation: $%E = 100(C_0 - C)/C_0$, where $C_0 = 50$ ppm. The effect of pH was studied as well, as shown in (Fig. 6a). The extraction efficiency percentage of Cd^{2+} was found to increase in alkaline solution, the highest extraction efficiency percentages ($E = 93%$) were noted in alkaline solution a pH=8 under illumination. It is important to note that the solubility product of $Cd(OH)_2 = 7.2 \times 10^{-15} = [Cd^{2+}][OH^-]^2$, so knowing that the concentration of 50 ppm of $Cd(NO_3)_2$ is equivalent to 2.1×10^{-4} , at PH=8, $[Cd^{2+}][OH^-]^2 = [2.1 \times 10^{-4}] * [10^{-6}]^2 = 2.1 \times 10^{-16}$ which is less than the Ksp of $Cd(OH)_2$, based on this $Cd(OH)_2$ will never precipitate at This PH=8 [60]. This was also confirmed by ICP where the concentrations at different pH values were the same.

Figure 6b shows the trends of extraction efficiency at different periods of time for Cd^{2+} using CH, and CH-CDs under dark and light at pH=8. As shown after 6 min only, the CH-CDs sample reached the maximum

extraction efficiency (93%) under UV-light irradiation, while the CH-CDs under dark and the pristine reached 80 and 61%, respectively. It is important to note that the kinetics of Cd^{2+} removal was very fast; the maximum extraction efficiency percentages for the CH-CDs membranes was reached after 3 min only under UV irradiation at pH=8 and it is five times faster than CH-CDs under dark conditions.

Adsorption kinetics and isotherm

To describe the adsorption of Cd^{2+} onto CH-CDs, the first- and second-order kinetics models were applied as following; the first-order kinetics model is described by Eq. (2):

$$\ln(q_e - q_t) = \ln q_e - k_1 \times t. \tag{2}$$

The pseudo-second-order kinetic model can be described by the following equation:

$$t/q_t = 1/k_2q_e^2 + t/q_e. \tag{3}$$

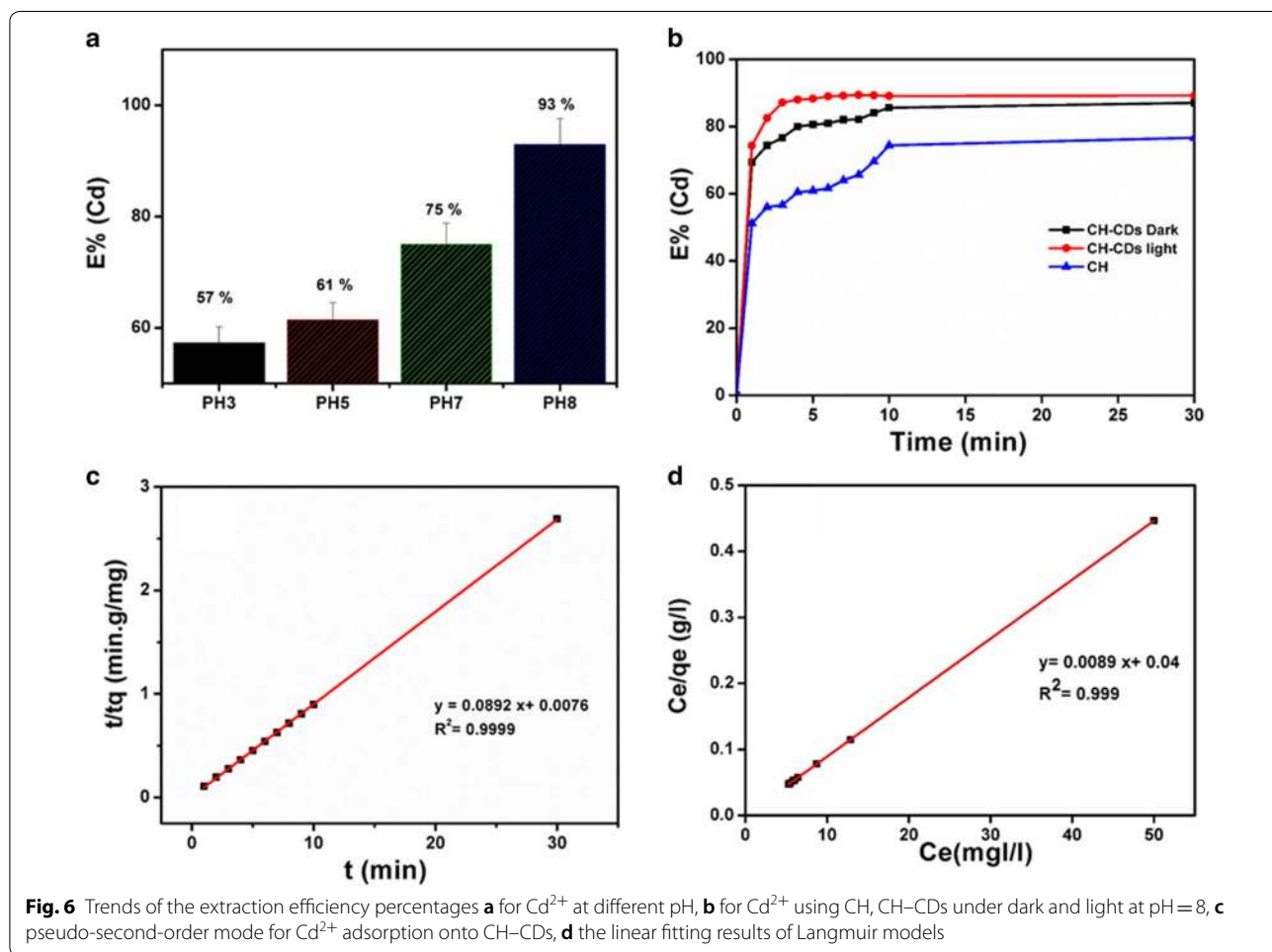


Fig. 6 Trends of the extraction efficiency percentages **a** for Cd^{2+} at different pH, **b** for Cd^{2+} using CH, CH-CDs under dark and light at pH = 8, **c** pseudo-second-order mode for Cd^{2+} adsorption onto CH-CDs, **d** the linear fitting results of Langmuir models

q_t and q_e (mg g^{-1}) are, respectively, the quantities of Cd^{2+} adsorbed at time t (min) and equilibrium. k_1 ($1/\text{min}$) present the rate constant of pseudo-first-order, and k_2 ($\text{g}(\text{mg min})^{-1}$) is the rate constant of pseudo-second-order models.

The adsorption data can be calculated using Langmuir or Freundlich models, through the following equations, respectively;

$$C_e/q_e = 1/K_L q_{\text{max}} + C_e/q_{\text{max}}, \tag{4}$$

$$\log q_e = \log K_f + 1/n \times \log C_e. \tag{5}$$

q_{max} is the maximum sorption capacity (mg g^{-1}), q_e is the solid phase equilibrium concentration and C_e is the equilibrium concentration of the metal ions (ppm) and K_L is a constant related to the binding energy of the sorption system (L mg^{-1}). The K_L and q_{max} can be deduced from the intercept and slope of the linear plots when C_e/q_e results in a properly line. Also, K_f and $1/n$ are associated to the Freundlich equilibrium constant K_f (mg g^{-1}) (mg L^{-1}) $^{1/n}$.

To evaluate the rate of Cd^{2+} removal on CH-CDs, the kinetics of the sorption model was applied. First-order and pseudo-second-order equations were used to study the variations in adsorption with time. The better correlation coefficient values were noted with pseudo-second-order model compared to the first-order kinetics (Fig. 6c, Table 1). From the above, the dominant mechanism could be chemical adsorption [61]. The adsorption isotherm is applied to estimate the adsorption capacity of an adsorbent. Moreover it gives a prediction, how the material interacts with adsorbents. Toward this end, the Langmuir and Freundlich isotherms [61] were used.

The adsorption isotherm, (Fig. 6d and Additional file 1: Figure S6) was conducted at constant pH=8 and RT. As concluded from Table 1, Fig. 6d and Additional file 1: Figure S6), Langmuir model was better fitted than Freundlich model based on the correlation coefficients (R^2). According to Freundlich model study, n values are slightly higher than one; this confirms that the sorption process might happen through electrostatic interaction, ion exchange, or combined mechanism [62].

Mechanism

Efficiency toward heavy metal removal could be arisen from chitosan coating, as previously reported [63], it could be concluded that a decrease in Cd^{2+} concentration in the presence of the pristine (pure chitosan) (Fig. 6b) happened because of the free NH_3^+ groups were again deprotonated due to the addition of NaOH. The deprotonated NH_2 groups from chitosane.

The deprotonated NH_2 groups from chitosan chelates with Cd^{2+} as per the already reported model [64]; however, for the CH-CDs membranes, some synergetic effect toward Cd^{2+} removal was observed. In addition to the chelating properties of chitosan, the well-dispersed CDs are doped with oxygen, nitrogen and sulfur, which exacerbates their chelating properties. Different mechanisms have been suggested to explain the interactions of heavy metals with carbon materials, doped with nitrogen and sulfur. Recent studies show that N and S dopants on the carbon dots surface increase the negative charge density of the carbon surface, and then enhance the ability for the Cd^{2+} removal compared to the non-doped carbon materials [65]. Based on Pearson theory, the affinity of heavy metals towards nitrogen/sulfur is explained by soft acid-soft base interactions, where, the CH-CDs act as soft base and Cd^{2+} as soft acids [66-68]. Moreover, another probable mechanism can be added based on the principle of ion exchange, indeed, Na^+ ions present in the CH membrane after dipping in NaOH solution (Fig. 7) stay bounded to the negatively charged CDs surface (Fig. 7), which are present in the chitosan film as previously described. The Na^+ ions from the hybrid (CH-CDs) membrane are released into the solution, and ion exchange Cd^{2+} ions are absorbed into the prepared membrane [46].

After the solution containing the (CH-CDs) and Cd^{2+} (50 mg L^{-1}) was irradiated by UV light (365 nm) for 30 min, removal of Cd^{2+} was almost complete (ca. 93%). Figure 6b plots the $E\%$ of Cd^{2+} versus reaction time, from which we can observe that the process of photo adsorption is ultra fast and efficient. Such a high adsorption activity of CH-CDs may be attributed to N and S dopants which reducing the band gap energy, delay the electron-hole recombination and enhance the light absorption

Table 1 Rate constants of the pseudo-first-order and pseudo-second-order kinetics models for the adsorption of Cd^{2+} on CH-CDs

Adsorbent	Pseudo-second order			Langmuir constants			Freundlich constants		
	q_e (mg g^{-1})	k_2 ($\text{g}(\text{mg min})^{-1}$)	R^2	K_L (L mg^{-1})	q_m (mg g^{-1})	R^2	K_f (mg g^{-1})(mg L^{-1}) $^{1/n}$	n	R^2
Cd^{2+}	10.23	1.13	0.9999	2.32	112.35	0.999	0.58	1.02	0.975

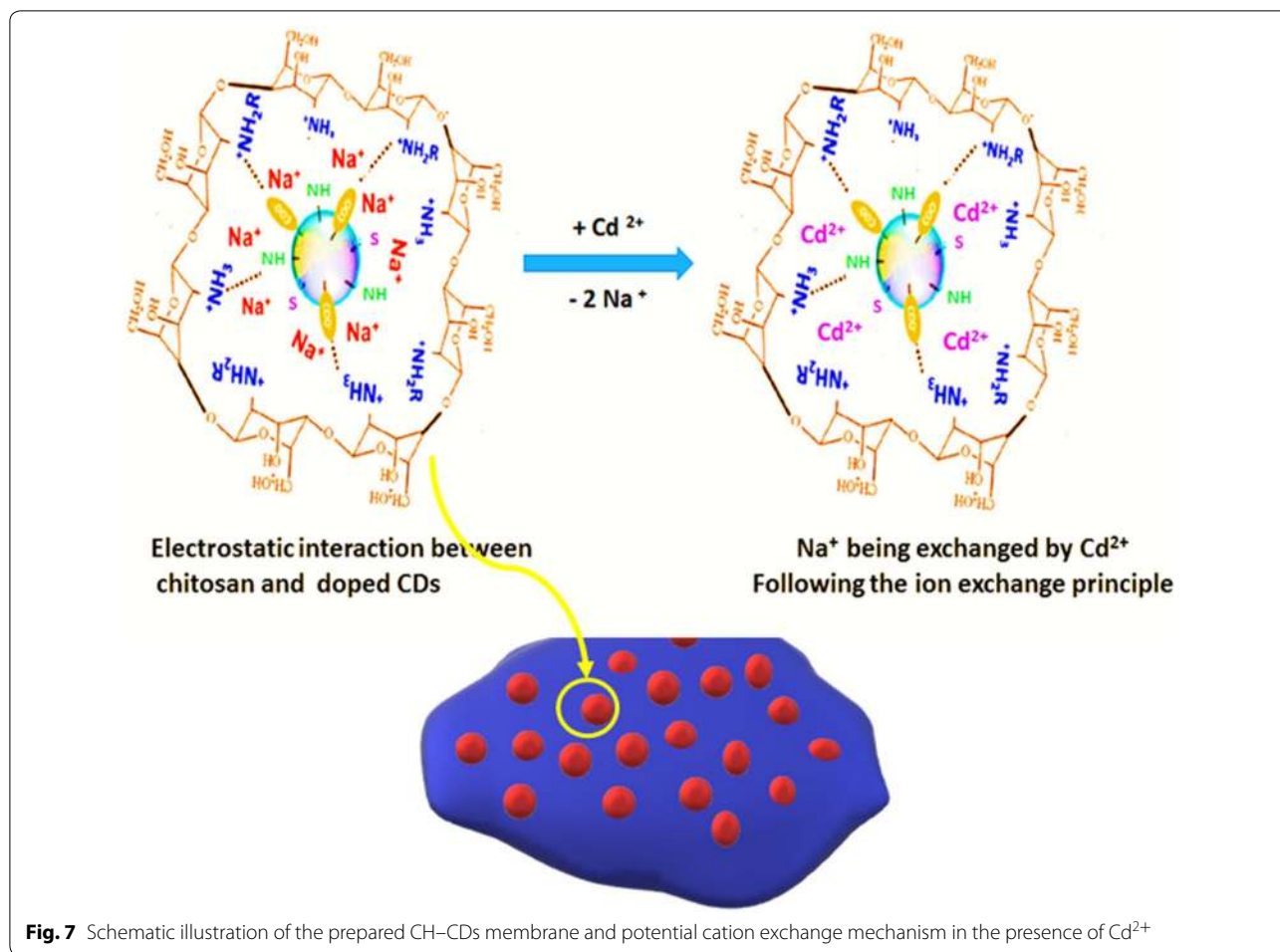


Table 2 Summary of some adsorbent-based carbon quantum dots used for Cd(II) removal

Adsorbent	$q_m/mg\ g^{-1}$	Experimental conditions	t/min	Refs.
SnO ₂ quantum dots decorated reduced graphene oxide	40.81	pH=6.5, 30 °C	20	[71]
Carbon quantum dots/layered double hydroxide	12.6	pH=6, T=30 °C	20	[9]
Carbon dots modified mesoporous organosilica	105.5	pH=8, T=30 °C	500	[72]
Poly (acrylic acid)-activated carbon nanocomposite	473.2	pH=6, T=25 °C	120	[73]
Hollow calcite single crystals with carbon quantum dots	66.68	pH=5, T=25 °C	90	[74]
S,N codoped carbon quantum dots modified chitosan membranes	112.4	pH=8 T=25 °C UV=365 nm	3	This work

of CDs results in increasing the electron density and enhancing the adsorption of positively charged Cd²⁺ [69, 70]. Nevertheless, the mechanism has not been fully explained and further study is needed. Results obviously demonstrated that N,S codoped CDs might enhance the UV-assisted adsorption efficiency towards Cd²⁺.

Comparison with other adsorbents

Previous works were summarized in Table 2 to compare our prepared material with the previously reported adsorbent. The time of adsorption under UV illumination was faster than others (5 min incubation). The optimal pH of the solution was 8, which is close to neutral

conditions. The optimal pH of the solution was 8, which is close to neutral conditions.

Conclusions

Novel photoluminescent CDs were produced from petroleum coke waste by hydrothermal simple method. The as-made CDs are rich in oxygen, nitrogen, and sulfur functional groups and high yield of monodispersed sub-5 nm CDs, outstanding water solubility and sensitive to pH in a wide range of 1–14. The as-prepared CDs were successfully introduced into the chitosan polymer matrix and form well-dispersed CH–CD fluorescent films. The latter are promising platforms for the removal of Cd²⁺ from industrial wastewater for a current project. The CH–CDs membranes show relatively good mechanical properties, based on stress-resistant. Interestingly, the UV-light illuminations, enhanced the Cd²⁺ removal efficiency of the photoluminescent CDs substantially five times faster under and the adsorption process could be described using pseudo-second-order kinetics and Langmuir isotherm model. The equilibrium time of adsorption was ultra fast (only 5 min). In addition, the optimal pH of the solution was 8 which is close to neutral. The maximum adsorption capacity at RT was found to be 112.4 mg g⁻¹ at pH 8. This work opens new avenues for producing low cost and rapid separation for practical adsorbent films based on green and low-cost fluorescent carbon quantum dots.

Supplementary information

Supplementary information accompanies this paper at <https://doi.org/10.1186/s12302-020-0292-z>.

Additional file 1. Additional tables and figures.

Abbreviations

CDs: carbon dots; CH: chitosan; AFM: atomic force microscopy; XPS: X-ray photoelectron; FTIR: Fourier-transform infrared; UV/Vis: ultraviolet/visible spectroscopy; (ICP) technique: inductive coupled plasma; q_{\max} : the maximum sorption capacity (mg g⁻¹); q_e : is the solid phase equilibrium concentration; C_e : the equilibrium concentration of the metal ions (ppm); K_L : constant related to the binding energy of the sorption system (L mg⁻¹); C_i and C_e (ppm): initial and equilibrium concentration of Cd²⁺; M (g): the mass of adsorbent; V (L): the volume of solution.

Acknowledgements

Open access funding provided by the Qatar National Library. The statements made herein are solely the responsibility of the authors.

Authors' contributions

KJ conceived the idea and contributed to the interpretation of data, and wrote the manuscript. MHS and KE designed experiments and data analysis, MMC contributed with the surface chemistry added effect. AMA and IK conceived the project and contributed to the writing of the manuscript. All authors reviewed the manuscript. All authors read and approved the final manuscript.

Funding

The NPRP [8-878-1-172] and UREP [25-091-2-034] awards, made this manuscript possible from Qatar National Research Fund (a member of Qatar Foundation).

Availability of data and materials

The datasets obtained and analyzed in the current study are available from the corresponding author on reasonable request.

Ethics approval and consent to participate

Not applicable.

Consent for publication

Not applicable.

Competing interests

The authors declare that they have no competing interests.

Received: 24 October 2019 Accepted: 17 January 2020

Published online: 05 February 2020

References

- Ozbey-Unal B, Imer DY, Keskinler B, Koyuncu I (2018) Boron removal from geothermal water by air gap membrane distillation. *Desalination* 433:141–150
- Attia H, Alexander S, Wright CJ, Hilal N (2017) Superhydrophobic electrospun membrane for heavy metals removal by air gap membrane distillation (AGMD). *Desalination* 420:318–329
- Mishra S et al (2019) Environmental biotechnology: for sustainable future. Springer, Berlin, pp 103–125
- Yu X, Cui W, Zhang F, Guo Y, Deng T (2019) Removal of iodine from the salt water used for caustic soda production by ion-exchange resin adsorption. *Desalination* 458:76–83
- Spahis N, Addoun A, Mahmoudi H, Ghaffour N (2008) Purification of water by activated carbon prepared from olive stones. *Desalination* 222:519–527
- Pérez-Botella E, Palomino M, Valencia S, Rey F (2019) Nanoporous materials for gas storage. Springer, Berlin, pp 173–208
- Jlassi K et al (2018) Bentonite-decorated calix [4] arene: a new, promising hybrid material for heavy-metal removal. *Appl Clay Sci* 161:15–22
- Yang X, Wan Y, Zheng Y, He F, Yu Z, Huang J, Wang H, Ok YS, Jiang Y, Gao B (2019) Surface functional groups of carbon-based adsorbents and their roles in the removal of heavy metals from aqueous solutions: a critical review. *Chem Eng J* 366:608–621. <https://doi.org/10.1016/j.cej.2019.02.119> (ISSN 1385-8947)
- Rahmanian O, Dinari M, Abdolmaleki MK (2018) Carbon quantum dots/layered double hydroxide hybrid for fast and efficient decontamination of Cd (II): the adsorption kinetics and isotherms. *Appl Surf Sci* 428:272–279
- Singh R et al (2018) QPRTase modified N-doped carbon quantum dots: a fluorescent bioprobe for selective detection of neurotoxin quinolinic acid in human serum. *Biosens Bioelectron* 101:103–109. <https://doi.org/10.1016/j.bios.2017.10.017>
- Baker SN, Baker GA (2010) Luminescent carbon nanodots: emergent nanolights. *Angew Chem Int Ed* 49:6726–6744
- Zuo J et al (2015) Preparation and application of fluorescent carbon dots. *J Nanomater*. <https://doi.org/10.1155/2015/787862>
- Wang L et al (2016) High-yield synthesis of strong photoluminescent N-doped carbon nanodots derived from hydrosoluble chitosan for mercury ion sensing via smartphone APP. *Biosens Bioelectron* 79:1–8. <https://doi.org/10.1016/j.bios.2015.11.085>
- Gao WL et al (2018) Carbon dots with red emission for sensing of Pt²⁺, Au³⁺, and Pd²⁺ and their bioapplications in vitro and in vivo. *ACS Appl Mater Interfaces* 10:1147–1154. <https://doi.org/10.1021/acsami.7b16991>

15. Lqbal A et al (2018) Heterogeneous synthesis of nitrogen-doped carbon dots prepared via anhydrous citric acid and melamine for selective and sensitive turn on-off-on detection of Hg(II), glutathione and its cellular imaging. *Sens Actuatur B Chem* 255:1130–1138. <https://doi.org/10.1016/j.snb.2017.08.130>
16. Mallakpour S, Behranvand V (2018) Synthesis of mesoporous recycled poly (ethylene terephthalate)/MWNT/carbon quantum dot nanocomposite from sustainable materials using ultrasonic waves: application for methylene blue removal. *J Clean Prod* 190:525–537
17. Scalbi S, Fantin V, Antolini F (2017) Environmental assessment of new technologies: production of a quantum dots-light emitting diode. *J Clean Prod* 142:3702–3718
18. Bao YW, Hua XW, Li YH, Jia HR, Wu FG (2018) Hyperthermia-promoted cytosolic and nuclear delivery of copper/carbon quantum dot-crosslinked nanosheets: multimodal imaging-guided photothermal cancer therapy. *ACS Appl Mater Interfaces* 10:1544–1555. <https://doi.org/10.1021/acsami.7b15332>
19. Sharma S, Dutta V, Singh P, Raizada P, Rahmani-Sani A, Hosseini-Bandegharaei A, Thakur VK (2019) Carbon quantum dot supported semiconductor photocatalysts for efficient degradation of organic pollutants in water: a review. *J Clean Prod* 228:755–769. <https://doi.org/10.1016/j.jclepro.2019.04.292> (ISSN 0959-6526)
20. Guan Y-F, Zhang F, Huang B-C, Yu H-Q (2019) Enhancing electricity generation of microbial fuel cell for wastewater treatment using nitrogen-doped carbon dots-supported carbon paper anode. *J Clean Prod* 229:412–419
21. Zuo PL, Lu XH, Sun ZG, Guo YH, He H (2016) A review on syntheses, properties, characterization and bioanalytical applications of fluorescent carbon dots. *Microchim Acta* 183:519–542. <https://doi.org/10.1007/s00604-015-1705-3>
22. Shastri LA, Kailasa SK, Wu HF (2009) Cysteine-capped ZnSe quantum dots as affinity and accelerating probes for microwave enzymatic digestion of proteins via direct matrix-assisted laser desorption/ionization time-of-flight mass spectrometric analysis. *Rapid Commun Mass Spectrom* 23:2247–2252. <https://doi.org/10.1002/rcm.4137>
23. Zhu HH et al (2016) One-step synthesis of graphene quantum dots from defective CVD graphene and their application in IGZO UV thin film phototransistor. *Carbon* 100:201–207. <https://doi.org/10.1016/j.carbon.2016.01.016>
24. Niu FS et al (2018) Electrochemically generated green-fluorescent N-doped carbon quantum dots for facile monitoring alkaline phosphatase activity based on the Fe³⁺-mediating ON-OFF-ON-OFF fluorescence principle. *Carbon* 127:340–348. <https://doi.org/10.1016/j.carbon.2017.10.097>
25. Lu YD et al (2018) Facile hydrothermal synthesis of carbon dots (CDs) doped ZnFe₂O₄/TiO₂ hybrid materials with high photocatalytic activity. *J Photochem Photobiol A Chem* 353:10–18. <https://doi.org/10.1016/j.jphotochem.2017.10.049>
26. Feng R-Q, Yuan Z-Y, Ren T-Z (2019) A facile hydrothermal method for preparation of fluorescent carbon dots on application of Fe³⁺ and fingerprint detection. *Methods Appl Fluoresc* 7:035001
27. Zhang XY et al (2018) Natural-product-derived carbon dots: from natural products to functional materials. *Chemosuschem* 11:11–24. <https://doi.org/10.1002/cssc.201701847>
28. Huang Y, Liao W (2019) Hierarchical carbon material of N-doped carbon quantum dots in situ formed on N-doped carbon nanotube for efficient oxygen reduction. *Appl Surf Sci* 495:143597
29. Tao W (2015) Managing China's petcoke problem
30. Acha Morrás ND, Elosúa Aguado C, Corres Sanz JM, Arregui San Martín FJ (2019) Fluorescent sensors for the detection of heavy metal ions in aqueous media. *Sensors* 19:599
31. Khan I et al (2017) polymeric nanocarriers: a new horizon for the effective management of breast cancer. *Curr Pharm Des* 23:5315–5326. <https://doi.org/10.2174/1381612823666170829164828>
32. Feng T, Ai XZ, An GH, Yang PP, Zhao YL (2016) Charge-convertible carbon dots for imaging guided drug delivery with enhanced in vivo cancer therapeutic efficiency. *ACS Nano* 10:4410–4420. <https://doi.org/10.1021/acs.nano.6b00043>
33. Feng HE et al (2018) Synthesis of three-dimensional porous reduced graphene oxide hydrogel/carbon dots for high-performance supercapacitor. *J Electroanal Chem* 808:321–328. <https://doi.org/10.1016/j.jelechem.2017.12.046>
34. Pacquiao MR, de Luna MDG, Thongsai N, Kladsomboon S, Paoprasert P (2018) Highly fluorescent carbon dots from enokitake mushroom as multi-faceted optical nanomaterials for Cr⁶⁺ and VOC detection and imaging applications. *Appl Surf Sci* 453:192–203
35. Wang L et al (2017) Visual in vivo degradation of injectable hydrogel by real-time and non-invasive tracking using carbon nanodots as fluorescent indicator. *Biomaterials* 145:192–206. <https://doi.org/10.1016/j.biomaterials.2017.08.039>
36. Liu G et al (2019) Rapid and high yield synthesis of carbon dots with chelating ability derived from acrylamide/chitosan for selective detection of ferrous ions. *Appl Surf Sci* 487:1167–1175
37. Jiang M et al (2018) Removal of heavy metal chromium using cross-linked chitosan composite nanofiber mats. *Int J Biol Macromol* 120:213–221
38. Zhang H et al (2019) A novel and biocompatible Fe₃O₄ loaded chitosan polyelectrolyte nanoparticles for the removal of Cd²⁺ ion. *Int J Biol Macromol* 141:1165–1174
39. Kumar P, Gihar S, Kumar B, Kumar D (2019) Synthesis and characterization of crosslinked chitosan for effective dye removal antibacterial activity. *Int J Biol Macromol* 139:752–759
40. Dutta PK, Dutta J, Tripathi V (2004) Chitin and chitosan: chemistry, properties and applications
41. Rao VN et al (2019) Sustainable hydrogen production for the greener environment by quantum dots-based efficient photocatalysts: a review. *J Environ Manag* 248:109246
42. Zhu L et al (2019) Metal-organic frameworks/carbon-based materials for environmental remediation: a state-of-the-art mini-review. *J Environ Manag* 232:964–977
43. Teow YH, Mohammad AW (2019) New generation nanomaterials for water desalination: a review. *Desalination* 451:2–17
44. Iram S et al (2012) Heavy metal tolerance of filamentous fungal strains isolated from soil irrigated with industrial wastewater. *Biologija* 58(3):107–116
45. Wu M et al (2014) Preparation of functionalized water-soluble photoluminescent carbon quantum dots from petroleum coke. *Carbon* 78:480–489
46. Baruah U, Konwar A, Chowdhury D (2016) A sulfonated carbon dot-chitosan hybrid hydrogel nanocomposite as an efficient ion-exchange film for Ca²⁺ and Mg²⁺ removal. *Nanoscale* 8:8542–8546
47. Li S et al (2014) Sulfur-doped graphene quantum dots as a novel fluorescent probe for highly selective and sensitive detection of Fe³⁺. *Anal Chem* 86:10201–10207
48. Zhu S et al (2013) Highly photoluminescent carbon dots for multicolor patterning, sensors, and bioimaging. *Angew Chem* 125:4045–4049
49. Tang L, Ji R, Li X, Teng KS, Lau SP (2013) Energy-level structure of nitrogen-doped graphene quantum dots. *J Mater Chem C* 1:4908–4915
50. Hong X et al (2017) Microstructuring of carbon/tin quantum dots via a novel photolithography and pyrolysis-reduction process. *Nano Res* 10:3743–3753
51. Mangione A et al (2005) Carbon nanocrystals produced by pulsed laser ablation of carbon. *Radiat Eff Defects Solids* 160:655–662
52. Chandra S et al (2013) Luminescent S-doped carbon dots: an emergent architecture for multimodal applications. *J Mater Chem B* 1:2375–2382
53. Ding H, Wei J-S, Xiong H-M (2014) Nitrogen and sulfur co-doped carbon dots with strong blue luminescence. *Nanoscale* 6:13817–13823
54. Rodrigues CV et al (2015) Down-and up-conversion photoluminescence of carbon-dots from brewing industry waste: application in live cell-imaging experiments. *J Braz Chem Soc* 26:2623–2628
55. Smith AM, Nie S (2009) Semiconductor nanocrystals: structure, properties, and band gap engineering. *Acc Chem Res* 43:190–200
56. Li Y et al (2011) Nitrogen-doped graphene quantum dots with oxygen-rich functional groups. *J Am Chem Soc* 134:15–18
57. Xia C et al (2019) An ultrafast responsive and sensitive ratiometric fluorescent pH nanoprobe based on label-free dual-emission carbon dots. *J Mater Chem C* 7:2563–2569
58. Fang B et al (2019) pH controlled green luminescent carbon dots derived from benzoxazine monomers for the fluorescence turn-on and turn-off detection. *J Colloid Interface Sci* 536:516–525
59. Sabet M, Mahdavi K (2019) Green synthesis of high photoluminescence nitrogen-doped carbon quantum dots from grass via a simple

- hydrothermal method for removing organic and inorganic water pollutants. *Appl Surf Sci* 463:283–291
60. Haynes WM (2014) *CRC handbook of chemistry and physics*. CRC Press, Boca Raton
 61. Messaoud-Bouregghda MZ (2019) Adsorption of heavy metals (cadmium, chrome and copper) on grafted cellulose: establishment of kinetic models. *Proc Int Acad Ecol Environ Sci* 9:53
 62. Almasri DA, Saleh NB, Atieh MA, McKay G, Ahzi S (2019) Adsorption of phosphate on iron oxide doped halloysite nanotubes. *Sci Rep* 9:3232
 63. Ahmad M, Ahmed S, Swami BL, Ikram S (2015) Adsorption of heavy metal ions: role of chitosan and cellulose for water treatment. *Langmuir* 79:109–155
 64. Krajewska B (2001) Diffusion of metal ions through gel chitosan membranes. *React Funct Polym* 47:37–47
 65. Cao Y et al (2016) One-pot melamine derived nitrogen doped magnetic carbon nanoadsorbents with enhanced chromium removal. *Carbon* 109:640–649
 66. Kiciński W, Szala M, Bystrzejewski M (2014) Sulfur-doped porous carbons: synthesis and applications. *Carbon* 68:1–32
 67. Pearson RG (1988) Absolute electronegativity and hardness: application to inorganic chemistry. *Inorg Chem* 27:734–740
 68. Wiśniewski M, Gauden P (2006) Pearson's hard-soft acid-base principle as a means of interpreting the reactivity of carbon materials. *Adsorpt Sci Technol* 24:389–402
 69. Guo Y, Cao F, Li Y (2018) Solid phase synthesis of nitrogen and phosphor co-doped carbon quantum dots for sensing Fe^{3+} and the enhanced photocatalytic degradation of dyes. *Sens Actuators B Chem* 255:1105–1111
 70. Li H et al (2010) Water-soluble fluorescent carbon quantum dots and photocatalyst design. *Angew Chem Int Ed* 49:4430–4434
 71. Dutta D, Thiyagarajan S, Bahadur D (2016) SnO_2 quantum dots decorated reduced graphene oxide nanocomposites for efficient water remediation. *Chem Eng J* 297:55–65
 72. Wang L et al (2015) Carbon dots modified mesoporous organosilica as an adsorbent for the removal of 2, 4-dichlorophenol and heavy metal ions. *J Mater Chem A* 3:13357–13364
 73. Ge H, Wang J (2017) Ear-like poly (acrylic acid)-activated carbon nanocomposite: a highly efficient adsorbent for removal of Cd (II) from aqueous solutions. *Chemosphere* 169:443–449
 74. Yang T et al (2018) Creation of hollow calcite single crystals with CQDs: synthesis, characterization, and fast and efficient decontamination of Cd (II). *Sci Rep* 8:17603

Publisher's Note

Springer Nature remains neutral with regard to jurisdictional claims in published maps and institutional affiliations.

Submit your manuscript to a SpringerOpen[®] journal and benefit from:

- Convenient online submission
- Rigorous peer review
- Open access: articles freely available online
- High visibility within the field
- Retaining the copyright to your article

Submit your next manuscript at ► [springeropen.com](https://www.springeropen.com)
